CDF note 8411

Search for Direct Pair Production of Scalar Top and Scalar Bottom Quarks in $p\bar{p}$ Collisions at $\sqrt{s} = 1.96$ TeV

The CDF Collaboration
URL http://www-cdf.fnal.gov
(Dated: July 24, 2006)

We report on the search for direct pair production of scalar top quarks and scalar bottom quarks using 295 pb^{-1} of proton-antiproton collision data recorded by the CDF experiment during Run 2 of the Tevatron. The scalar top (bottom) quarks are sought via their decay into a charm (bottom) quark and a neutralino, which is the lightest supersymmetric particle. The event signature is missing transverse energy and two high-$E_{\rm T}$ jets. In the signal regions the number of observed events are consistent with the number of events expected from Standard Model processes. Thus no evidence for scalar top quark nor scalar bottom quark is observed. 95% CL. limits are set on the cross section times squared branching ratio as function of the mass of scalar top quark and scalar bottom quark, for several neutralino masses, and we extended the exclusion region in the scalar top (bottom) quark mass versus neutralino mass plane. We assume 100% branching ratio for scalar top quark decays into charm quark and neutralino, and 100% branching ratio for scalar bottom quark decays into bottom quark and neutralino.

Preliminary Results for Summer 2006 Conferences

I. INTRODUCTION

Supersymmetry (SUSY) [1] is one of the most popular extensions to the Standard Model (SM) of particle physics. It overcomes some of the theoretical problems in the SM by introducing new degrees of freedom. In this model a scalar supersymmetric partner is assigned to every SM fermion, and a fermionic superpartner to every SM boson. Therefore the SM quark helicity states q_L and q_R aquire scalar partners $\tilde{q}_L$ and $\tilde{q}_R$. The mass eigenstates of each scalar quark is a mixture of its weak eigenstates. The amount of splitting of the mass eigenvalues depends on several factors. In the case of scalar top quark (stop), due to the large top quark mass and the large value of its Yukawa coupling constant (Higgs-to-top coupling), there is a significant split in the mass between the two mass eigenstates $\tilde{t}_1$ and $\tilde{t}_2$. In the case of scalar bottom quark (sbottom), large splitting of the two mass eigenstates $\tilde{b}_1$ and $\tilde{b}_2$ can occur at large $\tan\beta$. Thus it is likely that the lighter stop ($\tilde{t}_1$) quark and sbottom ($\tilde{b}_1$) quark can be much lighter compared to the light flavor squarks, and have relatively larger production cross sections at the Tevatron.

At the Tevatron, the stop and sbottom quarks are expected to be produced in pairs via gg fusion and $q\bar{q}$ annihilation. In this analysis, the stop quark is searched in the channel $p\bar{p} \to \tilde{t}_1\bar{\tilde{t}}_1 \to (c\tilde{\chi}_1^0)(\bar{c}\tilde{\chi}_1^0)$, and the sbottom quark is searched in the channel $p\bar{p} \to \tilde{b}_1\bar{\tilde{b}}_1 \to (b\tilde{\chi}_1^0)(\bar{b}\tilde{\chi}_1^0)$. The lightest neutralino $\tilde{\chi}_1^0$ is assumed to be the lightest supersymmetric particle and stable. This leads to experimental signatures with appreciable missing transverse energy. The decay $\tilde{t}_1 \to c\tilde{\chi}_1^0$ dominates via a one-loop diagram in the absence of flavor-changing neutral currents if $m_{\tilde{t}_1} < m_b + m_{\chi_1^\pm}$, $m_{\tilde{t}_1} < m_W + m_b + m_{\chi_1^0}$, $m_{\tilde{t}_1} < m_b + m_{\tilde{\nu}}$, and $m_{\tilde{t}_1} < m_b + m_{\tilde{l}}$. For these two searches we assume $BR(\tilde{t}_1 \to c\tilde{\chi}_1^0) = 100\%$ and $BR(\tilde{b}_1 \to b\tilde{\chi}_1^0) = 100\%$. The signature of the process in these two searches is a pair of acolinear heavy flavor jets in the transverse plane, large $\not\!\!E_{\rm T}$, and no isolated high $p_{\rm T}$ leptons in the final state. In this search we use 295 ± 18 pb^{-1} [2] of $p\bar{p}$ collision data at a center-of-mass energy of 1.96 TeV recorded by the Collider Detector at Fermilab (CDF) during the Tevatron Run II.

CDF is a general-purpose detector that is described in detail elsewhere [3]. The components relevant to this analysis are briefly described here. The charged-particle tracking system is closest to the beam pipe, and consists of multi-layer silicon detectors (SVX) [4] and a large open-cell drift chamber covering the pseudorapidity region $|\eta| < 1$ [5]. The silicon detectors allow a precise measurement of a track's impact parameter with respect to the primary vertex in the plane transverse to the beam direction. The tracking system is enclosed in a superconducting solenoid, which in turn is surrounded by a calorimeter. The CDF calorimeter system is organized into electromagnetic and hadronic sections segmented in projective tower geometry, and covers the region $|\eta| < 3.6$. The electromagnetic calorimeters utilize a lead-scintillator sampling technique, whereas the hadron calorimeters use iron-scintillator technology. The central muon-detection system, used for this analysis, is located outside of the calorimeter and covers the range $|\eta| < 1$.

II. DATA SAMPLE, EVENT SELECTION & BACKGROUNDS

In this analysis the $\not\!\!E_{\rm T}$ [5] is defined as the energy imbalance in the plane transverse to the beam direction. A jet is defined as a localized energy deposition in the calorimeter and is reconstructed using a cone algorithm with fixed radius $\Delta R \equiv \sqrt{\Delta\eta^2 + \Delta\phi^2} = 0.4$ in $\eta - \phi$ space [6]. We correct [6] jet $E_{\rm T}$ measurements and $\not\!\!E_{\rm T}$ for detector effects.

The data sample for this analysis was collected using a $\not\!\!E_{\rm T}$ +jets trigger, which is distributed across three levels of online event selection. In the first and second levels of the trigger, $\not\!\!E_{\rm T}$ is required to be greater than 25 GeV and is calculated by summing over calorimeter trigger towers [7] with transverse energies above 1 GeV. At level-2 there should be at least two calorimeter energy clusters (jets) with $E_{\rm T} > 10$ GeV. At level-3 $\not\!\!E_{\rm T}$ is required to be greater than 35 GeV, and is recalculated using full calorimeter segmentation with a tower energy threshold of 100 MeV. We use events from the inclusive high-$p_{\rm T}$ μ samples to measure the trigger efficiency directly from data.

A fraction of events taken with the trigger mentioned in the above paragraph, are not from $p-\bar{p}$ collisions, but from beam halo and cosmic ray sources. To remove these events we examine the event electromagnetic fraction (F_{em}) and charged fraction (F_{ch}) [8]. We reject events that contain little energy in the electromagnetic section of the calorimeter or that have mostly neutral-particle jets, by requiring $F_{em} > 0.1$ and $F_{ch} > 0.1$. We also reject events if any of the jet in the event enters un-instrumented regions of the calorimeter.

The dominant backgrounds to the stop and sbottom searches in the jets and $\not\!\!E_{\rm T}$ signature are QCD multi-jet production, W and Z boson production in association with jets, top quark single and pair production, and production of di-boson ($WW/WZ/ZZ$). The ALPGEN generator [9] was used for the simulation of the W and Z boson plus parton production, with HERWIG [10] used to model parton showers. The PYTHIA generator [11] is used to generate QCD multi-jet, top quark and di-boson productions. All these Monte Carlo SM background samples were generated using the CTEQ5L [12] parton distribution functions (PDF). In generating the QCD multi-jet sample, we only keep the events where there are b or c outgoing partons/hadrons in the final state (QCD multi-jet (HF)). To normalize the Monte Carlo SM background samples, we use the next-to-leading order (NLO) cross section values for top quark

(single/pair) production [13][14][15]. We use MCFM [16][17] program to obtain the NLO cross section values for W/Z+jets and di-boson productions. For QCD multi-jet (HF) sample, we select a kinematic region in the data that is dominated by QCD di-jet production, and obtain a normaization factor $k_{QCD} = 1.46 \pm 0.37$ for the QCD multi-jet (HF) sample. The uncertainty of the normaization factor is mainly due to the uncertainty of the jet energy scale.

Data selection requirements were chosen to maximize the statistical significance of the stop/sbottom signal over background events based on studies of simulated event samples before the signal region data were examined. As the production cross section and event kinematic (example jet $E_{\rm T}$, $\not\!\!E_{\rm T}$) could vary significantly across a wide stop quark and sbottom quark mass range to be searched, we determined separate sets of optimized cuts for three mass ranges for both stop and sbottom searches. The corresponding "low", "medium" and "high" mass ranges for stop (sbottom) search are $m_{\tilde{t}_1} < 100$ GeV, $100 \leq m_{\tilde{t}_1} < 120$ GeV, and $m_{\tilde{t}_1} \geq 120$ GeV ($m_{\tilde{b}_1} < 140$ GeV, $140 \leq m_{\tilde{b}_1} < 180$ GeV, and $m_{\tilde{b}_1} \geq 180$ GeV). To select the events, we require the missing transverse energy to be $\not\!\!E_{\rm T} > 50$ GeV or higher, to be in the region that the trigger is efficient, and to reduce QCD multi-jet background. In each selected event we require there to be only two or three reconstructed jets in the rapidity region $|\eta| < 2$. Events with any additional jets with $E_T > 8$ GeV and $2 < |\eta| < 3.6$ are rejected. To reject events with $\not\!\!E_{\rm T}$ resulting from jet energy mis-measurement, we require that the opening angle in the transverse plane between the two highest E_T jets satisfy $\Delta\phi(j_1, j_2) < 160°$. The $\not\!\!E_{\rm T}$ direction must not be parallel to any of the jets. We require the minimum azimuthal separation between the direction of the jets and $\not\!\!E_{\rm T}$ of $\min \Delta\phi(j, \not\!\!E_{\rm T}) > 45°$. In QCD multi-jet events, most of the time the missing transverse energy is due to mis-measurement of jets' energy. So it is often that the second leading jet's transverse energy is anti-correlated to the missing transverse energy. Therefore we require that the sum $E_{\rm T}({\rm Jet2}) + \not\!\!E_{\rm T}$ to be above certain cut values (shown in Table I). These criteria reject most of the QCD multi-jet background events.

To reduce the background contribution from W/Z+jets and top quark production, we reject events with one or more identified leptons with $E_T > 10$ GeV (electron candidates) or $p_{\rm T} > 10$ GeV/c (muon candidates), or with any isolated track $p_{\rm T} > 10$ GeV/c. Criteria similar to those in [19] are used to identify the leptons. To further reduce this background we require each jet not to be highly electromagnetic (jet electromagnetic fraction < 0.9). The number of tracks associated to the first and second leading jets should be 4 or more tracks. This cut is to reduce contributions from W+jets and Z+jets in which the gauge bosons decay into taus.

A quantity which explores the correlation between the missing transverse energy and the transverse energy of the first and second leading jets, $E^v_{\rm T_{J12MET}}$ [20], is required to be in the range $-10 < E^v_{\rm T_{J12MET}} < 10$ GeV, to reduce contributions from QCD multi-jet and top quark production.

To further enhance the signal over the SM background, we tag the c-jets (b-jets) in the stop (sbottom) quark search with a heavy-flavor jet tagging algorithm, Jet-Probability [18]. The Jet-Probability algorithm examines the impact parameter of the tracks that are associated to the jet, and compute the probability that the tracks of the jet are originated from the primary vertex. For jets that are originated from primary (secondary) vertex, it will have a large (small) Jet-Probability value. For the stop (sbottom) search, we require at least one jet to have a Jet-Probability value of $JP < 5\%$ ($JP < 1\%$). The efficiency to tag a fiducial c-jet (b-jet) with Jet-Probability value of $JP < 5\%$ ($JP < 1\%$) is $\sim 17\%$ ($\sim 40\%$).

A detail description of the selection cuts are shown in Table I.

Among the contributions from SM processes that pass all the selection cuts, some events are selected even though only light-flavor jets are present in the event final state. One or more light-flavor jets are mis-identified as a c-jet or b-jet by the Jet-Probability algorithm (mis-tag). So when we estimate the SM background contributions with Monte Carlo samples, we require that a heavy flavor parton/hadron to be matched to the jet before we cut on its Jet-Probability value. To estimate the fraction of selected SM events that are due to light-flavor jets mis-identifed as c or b-jets, we measured the rate of mis-tag on a data sample that is riched in light-flavor jets. We then apply this measured mis-tag rate onto the data sample that is used for the stop and sbottom searches, after all selection cuts are applied except the heavy flavor jet tagging.

III. SIGNAL ACCEPTANCE AND SYSTEMATIC UNCERTAINTIES

The total detection efficiencies for the stop and sbottom quark signals are estimated using the PYTHIA event generator, and the CDF detector simulation program. The PYTHIA underlying event simulation was tuned to reproduce CDF data [21]. The samples were generated using the CTEQ5L parton distribution functions, with the renormalization and factorization scales set to the mass of the squark in the search. The total stop (sbottom) efficiency in the accessible mass region vary from 0.1% to 3.4% (0.17% to 8.5%). The efficiency increases for higher stop (sbottom) mass and larger mass difference between $\tilde{t}_1$ ($\tilde{b}_1$) and $\tilde{\chi}^0_1$.

The systematic uncertainty on the signal acceptance includes the uncertainties due to modeling gluon radiation from the initial-state or final-state partons (5%), and the choice of the PDF (2%). The limited size of the stop and sbottom simulation samples gives a 2-10% statistical uncertainty. The signal acceptance uncertainty due to the jet

energy scale varies from 4% to 20%, and the uncertainty on the luminosity is 6%. The uncertainty on the trigger efficiency is 5%. The systematic uncertainty for tagging c-jet (b-jet) is 12% (8.6%).

IV. RESULTS

After applying all the selection cuts, the number of expected SM background events are consistent with the number of observed events for both the stop quark and sbottom quark searches. The break down of the SM contributions and the total number of observed data events for the stop (sbottom) quark search is listed in Table II (III). In both stop and sbottom searches, and among all the mass range search categories, the largest source of background are events where light-flavor jets mis-identified as c or b-jets. The QCD multi-jet (HF) background is the second largest source of SM background in the "low" mass search. However its contribution is largely suppressed by the tigther cuts employed in the "medium" and "high" mass searches. The plots in Figure 1 show the comparison of kinematic distributions between the observed data events and the SM background expectation, for "high" mass stop search after all selection cuts are applied. The solid open histograms are distributions from stop quark pair production ($M(\tilde{t}) = 120$ GeV, $M(\tilde{\chi}_1^0) = 50$ GeV) signal. The plots in Figure 2 show the comparison of kinematic distributions between the observed data events and the SM background expectation, for "medium" mass sbottom search after all selection cuts are applied. The solid open histograms are distributions from sbottom quark pair production ($M(\tilde{b}) = 160$ GeV, $M(\tilde{\chi}_1^0) = 80$ GeV) signal.

As the observed events in the data are consistent with the prediction from the SM background contribution, no evidence for stop quark or sbottom quark production is observed. We calculate the upper limit on the on the possible number of signal events at 95 % confidence level (C.L.) using a frequentist CL_s approach [22]. The plots of the upper limit cross section for stop quark pair production as function of stop quark mass, for $m_{\chi_1^0} = 50, 55, 60$ GeV, are shown in Figure 3. The plots of the upper limit cross section for sbottom quark pair production as function of sbottom quark mass, for $m_{\chi_1^0} = 60, 70, 80$ GeV, are shown in Figure 4. The theoretical cross sections for stop and sbottom quark pair production are calculated at NLO using Prospino [23] with CTEQ6M PDF. In the plots of Figure 3 and 4, the yellow band indicates the uncertainty of the theoretical cross section due to uncertainties in the PDF, and the renormalization and factorization scale.

The 95% CL exclusion region in the mass plane of $M(\tilde{t})$ ($M(\tilde{b})$) vs $M(\tilde{\chi}_1^0)$ is shown in Figure 5,6 (7,8). In Figure 5 (7) the uncertainties of the theoretical cross section due to PDF and renormalization and factorization scale are NOT taken into consideration when extracting the upper mass limit for CDF Run 2. In Figure 6 (8) the uncertainties of the theoretical cross section due to PDF and renormalization and factorization scale are taken into consideration when extracting the upper mass limit for CDF Run 2.

In conclusion, we performed searches for stop and sbottom quarks in the jets and $\not\!\!E_{\rm T}$ topology using 295 pb^{-1} of CDF Run II data. No evidence for stop quark nor sbottom quark is observed. We set an upper limit on their production cross section at the 95% C.L.

Acknowledgments

We thank the Fermilab staff and the technical staffs of the participating institutions for their vital contributions. This work was supported by the U.S. Department of Energy and National Science Foundation; the Italian Istituto Nazionale di Fisica Nucleare; the Ministry of Education, Culture, Sports, Science and Technology of Japan; the Natural Sciences and Engineering Research Council of Canada; the National Science Council of the Republic of China; the Swiss National Science Foundation; the A.P. Sloan Foundation; the Bundesministerium fuer Bildung und Forschung, Germany; the Korean Science and Engineering Foundation and the Korean Research Foundation; the Particle Physics and Astronomy Research Council and the Royal Society, UK; the Russian Foundation for Basic Research; the Comision Interministerial de Ciencia y Tecnologia, Spain; and in part by the European Community's Human Potential Programme under contract HPRN-CT-2002-00292, Probe for New Physics.

[1] H.P. Nilles, Phys. Rep. **110** (1984) 1;
H.E. Haber and G.L. Kane, Phys. Rep. **117** (1985) 75.
[2] S. Klimenko, J. Konigsberg and T. Liss, FERMILAB-FN-0741 (2003); D. Acosta *et al.*, Nucl. Instrum. Meth. **A494**, 57 (2002).
[3] CDF Collaboration, FERMILAB-PUB-96/390-E.

[4] A. Sill *et al.*, Nucl. Instrum. and Methods A **447**, 1 (2000).

[5] CDF uses a cylindrical coordinate system in which θ is the polar angle to the proton beam, ϕ is the azimuthal angle about the beam axis, and pseudorapidity is defined as $\eta = -\ln \tan(\theta/2)$. The transverse energy and transverse momentum are defined as $E_T = E\sin\theta$ and $p_T = p\sin\theta$, where E is energy measured in the calorimeter and p is momentum measured by the tracking system. The missing transverse energy vector, $\not\!\!E_{\rm T}$, is $-\sum_i E_T^i \boldsymbol{n}_i$, where $\boldsymbol{n}_i$ is the unit vector in the azimuthal plane that points from the beamline to the ith calorimeter tower.

[6] T. Affolder *et al.* (CDF Collaboration), Phys. Rev. **D64**, 032001 (2001).

[7] The physical calorimeter towers are organized into larger trigger towers, covering approximately 0.26 in $\Delta\phi$ and 0.22 in $\Delta\eta$.

[8] F_{em} is the ratio of the energy measured by the electromagnetic calorimeter to the total energy contained in jets of cone radius $\Delta R = 0.4$ with $E_T > 10$ GeV and $|\eta| < 3.6$. F_{ch} is the fraction of the jet energy carried by measured charged-particle tracks ($p_T > 0.5$ GeV/c) averaged over the central jets with $|\eta| < 0.9$. These variables are similar to ones used in T. Affolder *et al.* (CDF Collaboration), Phys. Rev. Lett. **88**, 041801 (2002).

[9] M.L. Mangano *et al.*, JHEP **07**, 001 (2003). We use version 1.2.

[10] G. Corcella *et al.*, JHEP **01**, 010 (2001); hep-ph/0210213. We use version 6.4a.

[11] T. Sjostrand, P. Eden, C. Friberg, L. Lonnblad, G. Miu, S. Mrenna and E. Norrbin, Computer Physics Commun. 135, 238 (2001), version 6.203.

[12] H. L. Lai *et al.* (CTEQ Collaboration), Eur. Phys. J. **C12** 375 (2000).

[13] M. Cacciari, S. Frixione, M.L. Mangano, P. Nason, and G. Ridolfi, "The $t\bar{t}$ Cross-Section at 1.8 TeV and 1.96 TeV: A Study of the Systematics Due to Parton Densities and Scale Dependence", 2003.

[14] B.W. Harris *et. al.*, Phys. Rev. D 66, 054024 (2002).

[15] Z. Sullivan, Fermilab-Pub-04-142-T, hep-ph/0408049

[16] J.M. Campbell, R.K. Ellis, Phys. Rev. D60:113006 (1999), hep-ph/9905386

[17] J.M. Campbell, R.K. Ellis, Phys. Rev. D65:113007 (2002), hep-ph/0202176

[18] A. Abulencia *et al.* (CDF Collaboration), FERMILAB-PUB-06-247-E, hep-ex/0607035, submitted to PRD

[19] D. Acosta *et al.* (CDF Collaboration), FERMILAB-PUB-04/051-E., accepted by Phys. Rev. Lett.

[20] The quantity $E^v_{\rm TJ12MET}$ is defined as follow : $\vec{E}_{\rm TJ12MET} = \vec{E}_{\rm TJ1} + \vec{E}_{\rm TJ2} + M\vec{E}T$ ($\vec{E}_{\rm TJ1}$ and $\vec{E}_{\rm TJ2}$ are, respectively, the vector of the transverse energy of the first and second leading jets, and $M\vec{E}T$ is the vector of the missing transverse energy), $\vec{E}_{\rm TJ12} = \vec{E}_{\rm TJ1} + \vec{E}_{\rm TJ2}$, $\vec{v} = \vec{E}_{\rm TJ12}/\mid \vec{E}_{\rm TJ12} \mid$, $E^v_{\rm TJ12MET} = \vec{E}_{\rm TJ12MET} \cdot \vec{v}$.

[21] T. Affolder *et al.* (CDF Collaboration), Phys. Rev. D **65** 092002 (2002).

[22] T. Junk, "Confidence Level Computation For Combining Searches With Small Statistics", Nucl. Instrum. Meth., A434, p. 435-443 (1999).

[23] W. Beenakker *et al.*, Phys. Rev. Lett. **83**, 3780 (1999);
T. Plehn http://pheno.physics.wisc.edu/~plehn/prospino/prospino.html.

Selection Cuts	Stop			Sbottom		
Mass range	Low	Medium	High	Low	Medium	High
Loose Lepton Veto	YES					
$\not\!\!E_{\rm T}$ (GeV)	> 50	> 50	> 50	> 50	> 55	> 65
$E_{\rm T}$ Jet 1 (GeV)	> 35	> 45	> 55	> 35	> 55	> 75
$E_{\rm T}$ Jet 2 (GeV)	> 15	> 15	> 25	> 15	> 15	> 35
$E_{\rm T}$ Jet 3 (GeV)	> 15					
Jet Rapidity ($\mid \eta \mid$: J1, J2, J3)	$\mid \eta_1 \mid < 1.2$, $\mid \eta_2 \mid < 1.5$, $\mid \eta_3 \mid < 2.0$					
Veto additional jets	$E_{\rm T} > 8$ GeV, $2 < \mid \eta \mid < 3.6$					
$\Delta\phi$(Jet1, Jet2) (deg)	$70 - 160$			$60 - 160$	$50 - 160$	$40 - 160$
min. $\Delta\phi$(Jet, $\not\!\!E_{\rm T}$) (deg)	$45 - 180$					
min. # tracks in jet ($\mid \eta \mid < 1$) (for Jet1, Jet2, or Jet3)	$>= 4$					
$Et^{\nu}_{\rm J12MET}$ (GeV)	< 15					
$E_{\rm T}$(Jet2) + $\not\!\!E_{\rm T}$ (GeV)	> 65	> 85	> 105	> 80	> 120	> 160
Jet Probability Tagging	$>= 1$ tag ($JP < 5\%$)			$>= 1$ tag ($JP < 1\%$)		

TABLE I: Event selection cuts.

TABLE II: The number of observed data events, and the number of expected events from various Standard Model sources in the stop signal region. The Monte Carlo statistical error is the first uncertainty shown, and the systematic error from other sources is the second.

Process	Events expected		
	Low	Medium	High
W + jets	$11.5 \pm 2.43 \pm 2.62$	$9.31 \pm 2.30 \pm 2.12$	$3.95 \pm 1.54 \pm 0.90$
Z + jets	$9.93 \pm 0.50 \pm 2.02$	$7.34 \pm 0.43 \pm 1.49$	$4.14 \pm 0.34 \pm 0.84$
Di-boson	$2.52 \pm 0.11 \pm 0.48$	$1.99 \pm 0.09 \pm 0.38$	$0.89 \pm 0.06 \pm 0.17$
Top	$5.23 \pm 0.19 \pm 0.82$	$4.90 \pm 0.19 \pm 0.77$	$3.93 \pm 0.17 \pm 0.62$
QCD	$32.5 \pm 5.20 \pm 8.11$	$17.9 \pm 4.00 \pm 4.47$	$2.55 \pm 1.47 \pm 0.64$
Mistag	$75.4 \pm 2.22 \pm 10.7$	$53.5 \pm 1.98 \pm 7.60$	$27.2 \pm 1.51 \pm 3.87$
Total	137 ± 15.8	94.9 ± 11.1	42.7 ± 5.28
Data	151	108	43

TABLE III: The number of observed data events, and the number of expected events from various Standard Model sources in the sbottom signal region. The Monte Carlo statistical error is the first uncertainty shown, and the systematic error from other sources is the second.

Process	Events expected		
	Low	Medium	High
W + jets	$5.50 \pm 1.15 \pm 1.16$	$1.53 \pm 0.55 \pm 0.32$	$0.51 \pm 0.36 \pm 0.11$
Z + jets	$5.95 \pm 0.36 \pm 1.10$	$2.66 \pm 0.25 \pm 0.49$	$1.02 \pm 0.16 \pm 0.19$
Top	$4.22 \pm 0.17 \pm 0.56$	$2.88 \pm 0.14 \pm 0.38$	$1.16 \pm 0.09 \pm 0.16$
QCD	$18.8 \pm 4.01 \pm 4.70$	$2.60 \pm 1.50 \pm 0.65$	$0^{+2.05}_{-0}$
Mistag	$20.5 \pm 0.63 \pm 2.30$	$8.09 \pm 0.47 \pm 0.91$	$1.98 \pm 0.25 \pm 0.22$
Total	55.0 ± 7.24	17.8 ± 2.31	$4.67^{+2.16}_{-0.67}$
Data	60	18	3

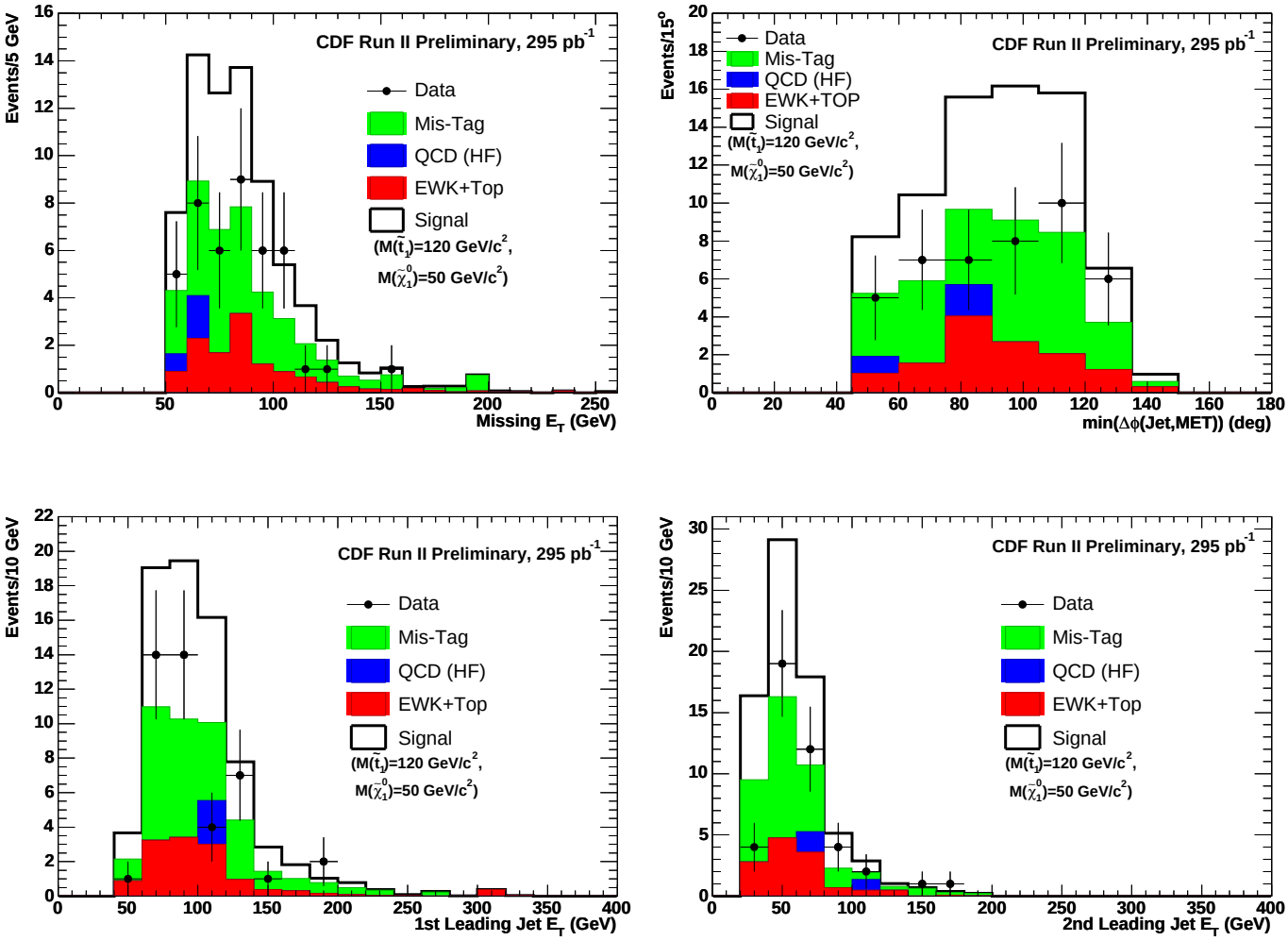

FIG. 1: Comparison of the kinematic distributions between the SM background prediction and data observation after applying **"high" mass cuts** in the search for **stop quark** pair production. (TOP LEFT) Missing transverse energy, (TOP RIGHT) minimum azimuthal angular separation between jet and MET, (BOTTOM LEFT) transverse energy of first leading jet, (MOTTOM RIGHT) transverse energy of second leading jet.

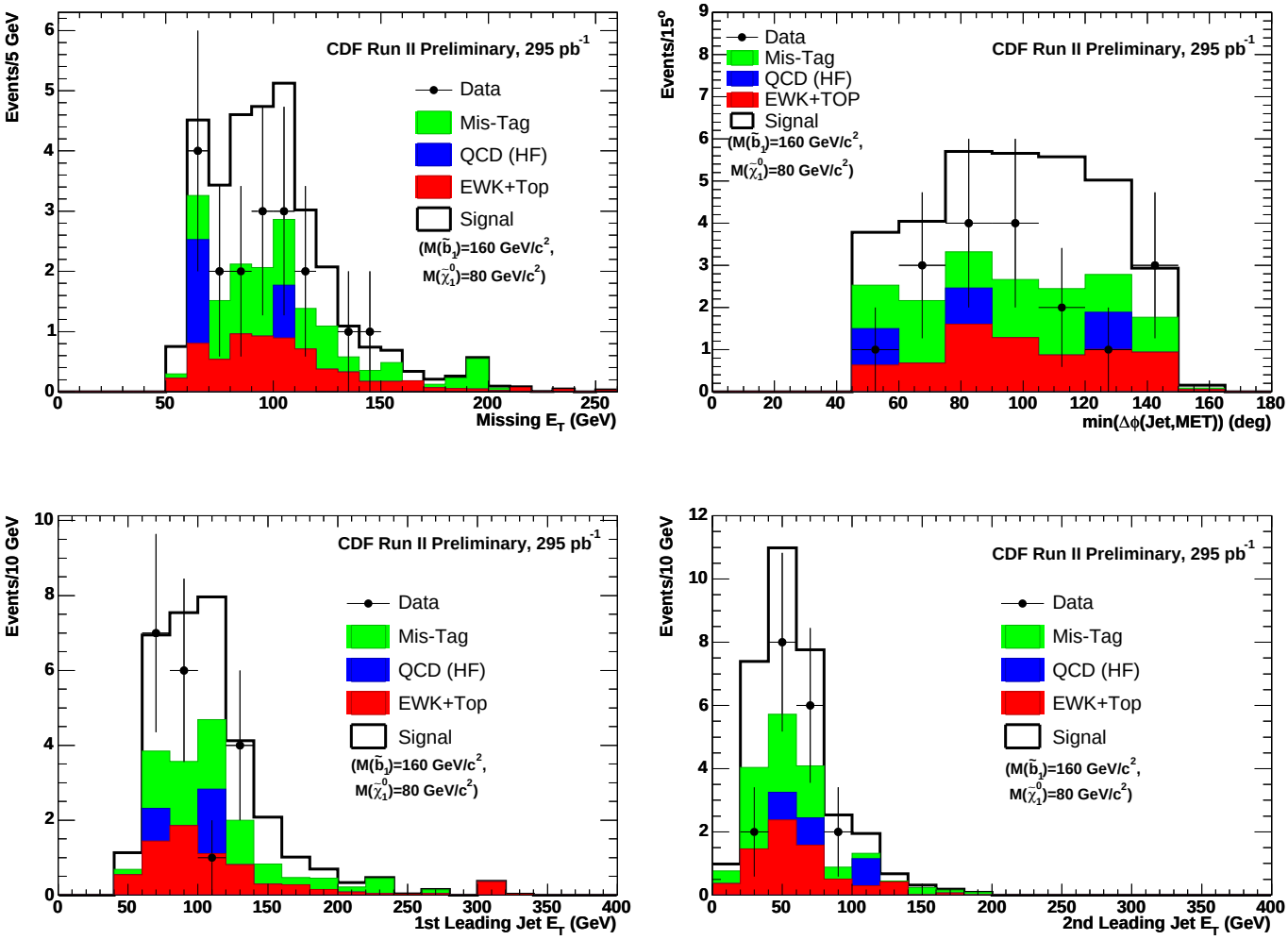

FIG. 2: Comparison of the kinematic distributions between the SM background prediction and data observation after applying **"medium" mass cuts** in the search for **sbottom quark** pair production. (TOP LEFT) Missing transverse energy, (TOP RIGHT) minimum azimuthal angular separation between jet and MET, (BOTTOM LEFT) transverse energy of first leading jet, (MOTTOM RIGHT) transverse energy of second leading jet.

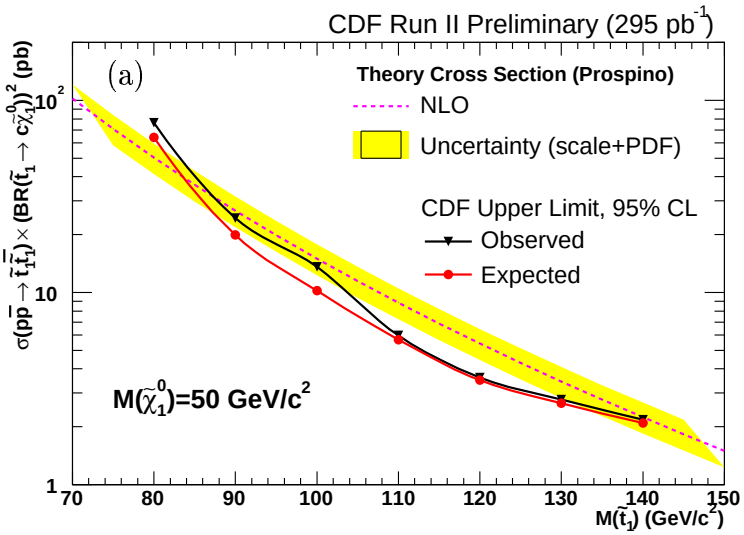

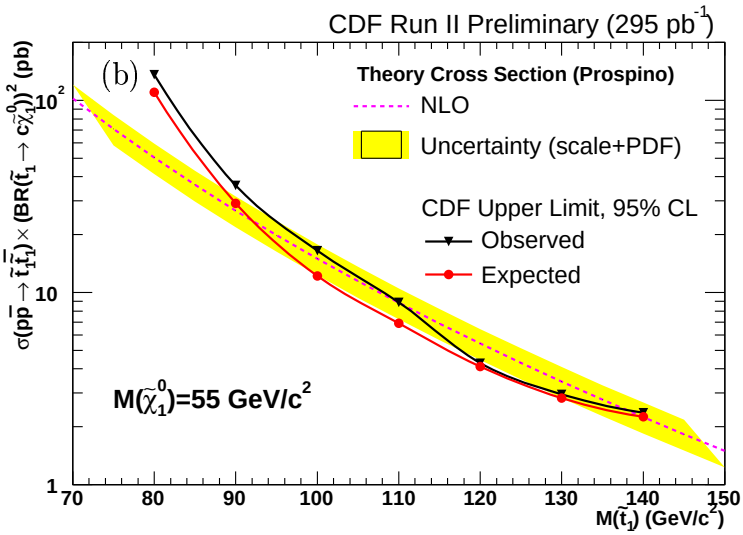

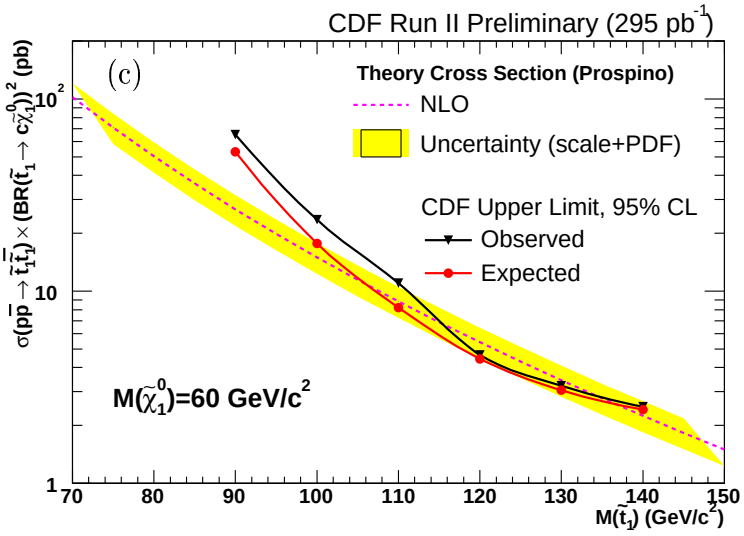

FIG. 3: The observed 95% C.L. upper limit on the pair production cross section of scalar top quarks for (a) $M(\tilde{\chi}_1^0) = 50$ GeV, (b) $M(\tilde{\chi}_1^0) = 55$ GeV, (c) $M(\tilde{\chi}_1^0) = 60$ GeV.

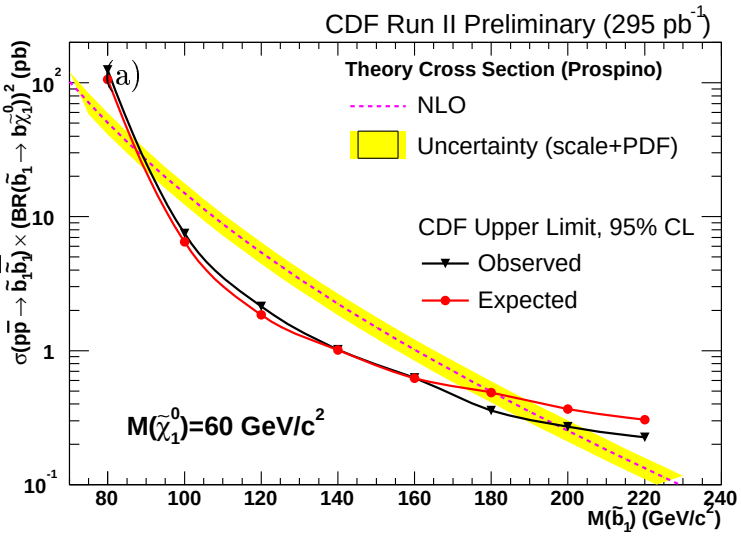

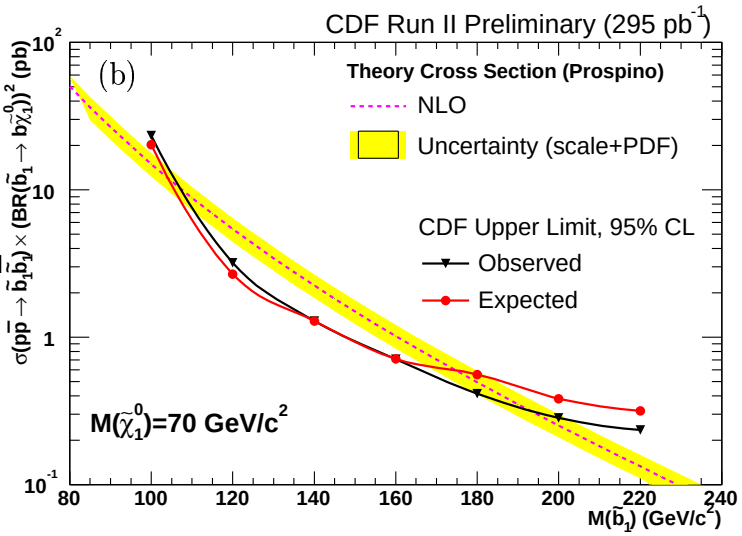

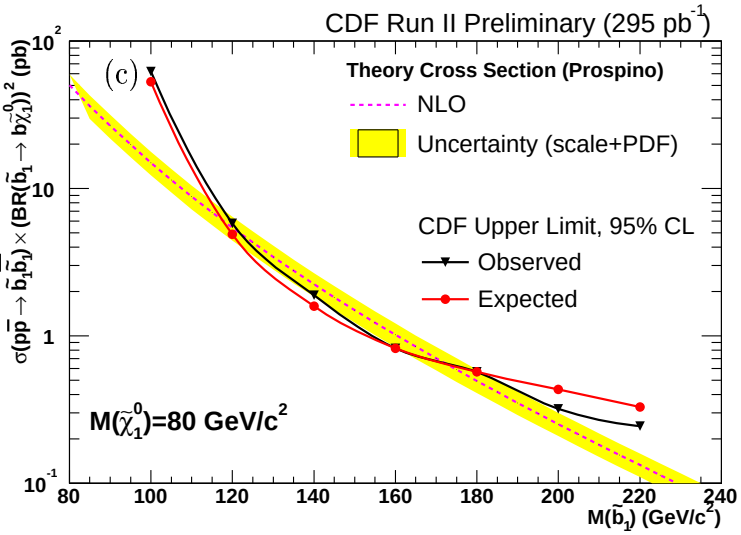

FIG. 4: The observed 95% C.L. upper limit on the pair production cross section of scalar bottom quarks for (a) $M(\tilde{\chi}_1^0) = 60$ GeV, (b) $M(\tilde{\chi}_1^0) = 70$ GeV, (c) $M(\tilde{\chi}_1^0) = 80$ GeV.

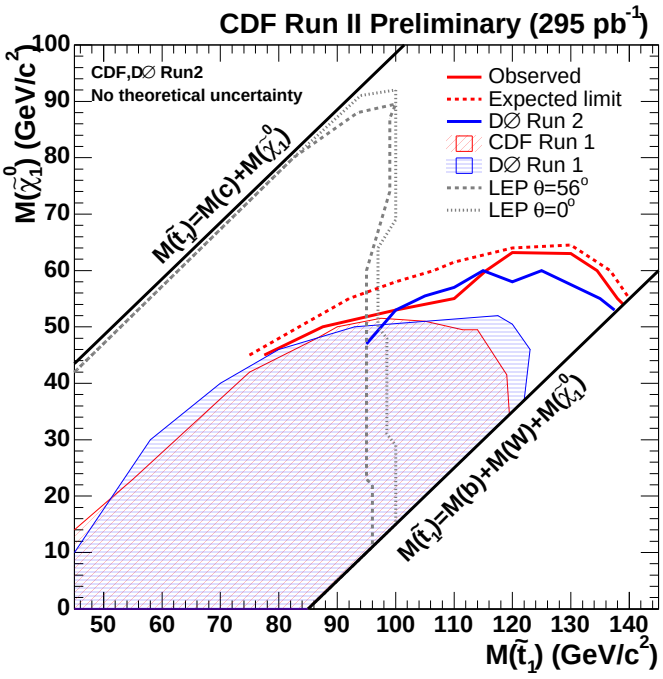

FIG. 5: The 95% CL exclusion region in the mass plane of $M(\tilde{t})$ vs $M(\tilde{\chi}_1^0)$. The upper mass limit from CDF and DØ Run2 does not include the uncertainties of the theoretical cross section due to PDF and renormalization and factorization scale.

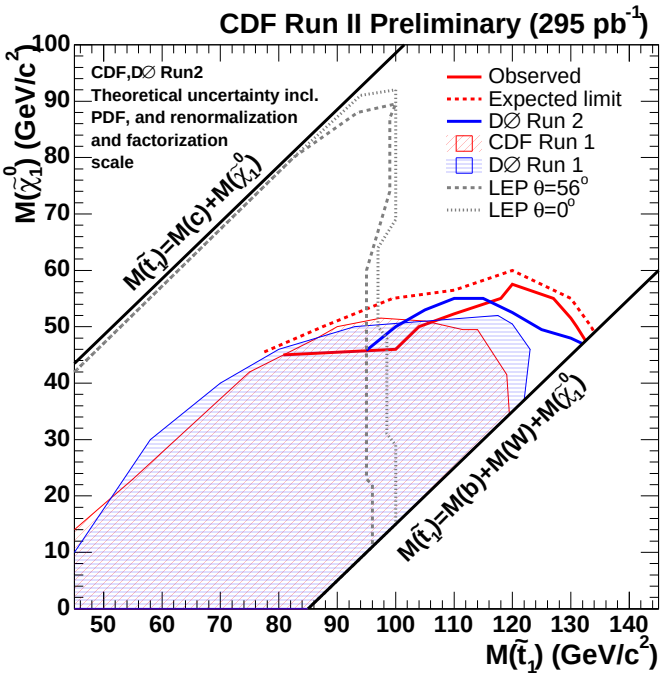

FIG. 6: The 95% CL exclusion region in the mass plane of $M(\tilde{t})$ vs $M(\tilde{\chi}_1^0)$. The upper mass limit from CDF and DØ Run2 includes the uncertainties of the theoretical cross section due to PDF and renormalization and factorization scale.

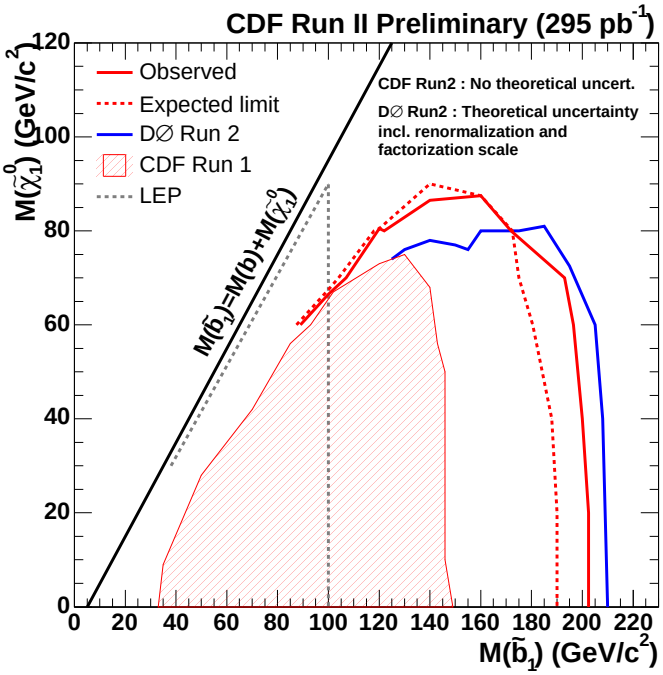

FIG. 7: The 95% CL exclusion region in the mass plane of $M(\tilde{b})$ vs $M(\tilde{\chi}_1^0)$. The upper mass limit from CDF Run2 does not include the uncertainties of the theoretical cross section due to PDF and renormalization and factorization scale.

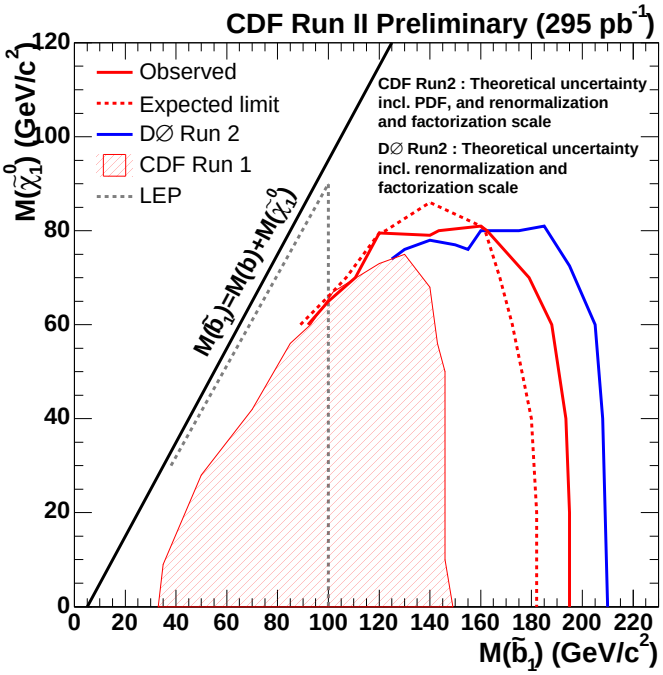

FIG. 8: The 95% CL exclusion region in the mass plane of $M(\tilde{b})$ vs $M(\tilde{\chi}_1^0)$. The upper mass limit from CDF Run2 includes the uncertainties of the theoretical cross section due to PDF and renormalization and factorization scale.